Hindawi Publishing Corporation
Journal of Sensors
Volume 2015, Article ID 470905, 12 pages
http://dx.doi.org/10.1155/2015/470905

Research Article

Deformation Monitoring of Geomechanical Model Test and Its Application in Overall Stability Analysis of a High Arch Dam

Baoquan Yang,[1] Lin Zhang,[1] Enlong Liu,[1] Jianhua Dong,[1] Honghu Zhu,[1,2] and Yuan Chen[1]

[1]*State Key Laboratory of Hydraulics and Mountain River Engineering, College of Water Resource & Hydropower, Sichuan University, Chengdu 610065, China*
[2]*School of Earth Sciences and Engineering, Nanjing University, Nanjing 210023, China*

Correspondence should be addressed to Yuan Chen; chenyuan8899@163.com

Received 16 November 2014; Revised 6 January 2015; Accepted 20 January 2015

Academic Editor: Fei Dai

Geomechanical model testing is an important method for studying the overall stability of high arch dams. The main task of a geomechanical model test is deformation monitoring. Currently, many types of deformation instruments are used for deformation monitoring of dam models, which provide valuable information on the deformation characteristics of the prototype dams. However, further investigation is required for assessing the overall stability of high arch dams through analyzing deformation monitoring data. First, a relationship for assessing the stability of dams is established based on the comprehensive model test method. Second, a stability evaluation system is presented based on the deformation monitoring data, together with the relationships between the deformation and overloading coefficient. Finally, the comprehensive model test method is applied to study the overall stability of the Jinping-I high arch dam. A three-dimensional destructive test of the geomechanical model dam is conducted under reinforced foundation conditions. The deformation characteristics and failure mechanisms of the dam abutments and foundation were investigated. The test results indicate that the stability safety factors of the dam abutments and foundation range from 5.2 to 6.0. These research results provide an important scientific insight into the design, construction, and operation stages of this project.

1. Introduction

Currently, the construction of high arch dams in China is undergoing vigorous development. Several high arch dams about 300 m high, which represent an advanced class of arch dams, are planned or under construction. For example, the Xiaowan arch dam (294.5 m high) was built on the Lancang River. The Jinping-I arch dam (305 m high) on the Yalong River is under construction. The Baihetan (289 m high) and Wudongde arch dams (265 m high) on the Jinsha River and the Songta arch dam (313 m high) on the Nujiang River are currently in the design phase. Most of them involve great dam heights and huge reservoir capacities. These large-scale arch dam projects are accompanied with large flood discharges, high earthquake intensities, and complicated geological conditions [1]. To guarantee the safety of these projects, it is important to study the stability of both arch dams and dam foundations, to select optimum foundation reinforcement schemes, and to evaluate the strengthening effects of the corresponding reinforcement measures. A lot of efforts have been made to monitor the field performance of dams [2], but the instrumentation costs are expensive and the interpretation of field monitoring results is complicated. Geomechanical model testing is an important approach that can solve these problems.

Geomechanical model testing is a method that can reasonably simulate the dam under investigation, by taking into account the geological structure of the dam abutment and its reinforcement measures using certain similarity principles [3, 4]. The primary purpose of this test is to obtain deformation characteristics and failure pattern of the prototype through overloading or strength reduction [5]. Using this method, the influences of the geological structure on the dam safety can be evaluated, which can provide a reference for designing foundation reinforcement schemes. In addition, by studying the deformation monitoring data and the failure mechanisms of dam abutments and foundations, the safety factor of the dam and foundation can be determined. Such monitoring

results are very intuitive for dam designers and decision makers.

Deformation monitoring is very important for geomechanical model tests. However, as the deformation of small-scale models is much smaller than the prototype, the deformation instruments should have very high precision. They should also have small sizes and light weights, so that they can be easily installed in the model dams. Currently, different types of deformation instruments, including mechanical sensors, inductive sensors, resistance strain gage, and differential transformers, are available. All of these instruments have been frequently used for deformation monitoring of geomechanical models and can meet the high-accuracy requirements. Due to the development of measurement technologies, especially the rapid development of computers and automation technologies, the measurement methods and techniques in model tests developed rapidly. These sensors are more accurate and reliable than conventional ones. For example, the internal displacement transducer developed by Zhang et al. [6] can be used to monitor the relative deformation of the structural planes in the rock mass. The small two-way resistance displacement sensor developed by Huang and Chen [7] can replace resistance strain gauges in the model instrumentation system. The fiber optic sensing method is another important advance for geomechanical model tests [8–10]. The fiber optic sensors have many advantages over conventional sensors, such as small size, high accuracy, and inherent resistance to corrosion and electrical noise [11–14].

Although the development of deformation testing techniques can meet the requirements of geomechanical model tests, more works should be conducted to relate the deformation measurements gained to the overall stability of high arch dams. Zhou et al. [15, 16], Liu et al. [17], and Zhang et al. [18] of Tsinghua University established an analysis and evaluation system for the model tests of several high arch dams in China, such as the Xianghongdian, Qingshiling, and Jinshuitan dams. They summarized the test results of these dams and grouped a set of safety evaluation methods based on λ_1 (initial cracking load), λ_2 (nonlinear start load), and λ_3 (limit fracture load) values. They also introduced the evaluation index into the engineering design specifications of China. Peng et al. [19] of Tongji University presented a systematic method for slope safety evaluation utilizing multisource monitoring information. However, a complete set of stability evaluation systems was not formed for the comprehensive test method of geomechanical models.

In this paper, a relationship for assessing the stability of dam safety is established based on the comprehensive model test method. A stability evaluation system is presented based on the deformation monitoring results. Two inflection points are proposed to indicate the stability condition of high arch dams. Finally, the comprehensive model test method was applied to study the overall stability of the Jinping-I high arch dam. A three-dimensional (3D) destructive test of a geomechanical model dam was conducted under reinforced foundation conditions. The deformation characteristics and failure mechanisms of the dam abutments and foundation were investigated in detail.

2. Comprehensive Test Method for Geomechanical Models

2.1. Principles of the Comprehensive Test Method. For geomechanical models, three test methods are widely used, including the overloading method, the strength reduction method, and the comprehensive method. The overloading method mainly considers the upstream overloading effect on the stability of the dam abutments. The strength reduction method focuses on the effects of the decreasing mechanical strengths of the rocks and weak structural planes in the abutments and foundation on the dam stability. The comprehensive method is a combination of the overloading and strength reduction methods, through which a variety of factors can be investigated within one model [20]. For the overloading method, multistage loadings are generally accomplished by using jacks installed on the upstream surface of the model dam, through which the water overloading is applied. The overloading method is extensively applied in geomechanical model tests because of its convenience. The comprehensive method can consider more factors simultaneously, but overloading and strength reduction must be conducted in one model, which results in a certain degree of difficulty. Here, we proposed a comprehensive test method for geomechanical models, which takes advantages of special temperature analogous materials [21–23].

The safety factor of the comprehensive test method was assessed by using the basic concepts of degree of safety (or the point safety factor) and the principles of the overloading method and the strength reduction method. The point safety factor can be expressed as follows:

$$K = \frac{(f \cdot N + c \cdot A)}{P} = \frac{\int (f \cdot \sigma + c)\, dA}{P} = \frac{\int \tau dA}{P}, \quad (1)$$

where K is the point safety factor, P is the design water pressure on the upstream dam surface (sliding force), f is the shear friction coefficient, c is the cohesion, N is the normal force of the sliding surface, A is the sliding surface area, σ is the normal stress on the surface of the integral infinitesimal, dA is the integral infinitesimal area, and τ is the shear strength at the surface of the integral infinitesimal.

Equation (1) can be rewritten as

$$1 = \frac{(f \cdot N + c \cdot A)}{K \cdot P} = \frac{\int (f \cdot \sigma + c)\, dA}{K \cdot P} = \frac{\int \tau dA}{K \cdot P}. \quad (2)$$

Equation (2) shows that in the overloading method the material mechanical parameters of f and c and the shear strength τ will remain constant. Thus, we can increase the design water pressure P until the model dam fails. The coefficient of the overload that corresponds to the failure of the model dam is called the overloading safety factor K.

Equation (2) can be rewritten as in the following format:

$$1 = \frac{(f \cdot N + c \cdot A)/K}{P} = \frac{\int [(f \cdot \sigma + c)/K]\, dA}{P} = \frac{\int (\tau/K)\, dA}{P}. \quad (3)$$

Equation (3) represents the concept of the strength reduction method. This method is under constant load conditions, but the mechanical parameters f and c of the rock mass and structural plane of the model gradually decrease in the test, until the model dam fails. The lowest coefficient of the mechanical parameters of the model materials in the model tests is called the strength reduction safety factor K.

If the K in (3) is decomposed into two parts, that is, the strength reduction coefficient K_1 and the overloading coefficient K_2, the following relationship can be obtained:

$$1 = \frac{(f \cdot N + c \cdot A)/K_1}{K_2 \cdot P} = \frac{\int [(f \cdot \sigma + c)/K_1]\, dA}{K_2 \cdot P} = \frac{\int (\tau/K_1)\, dA}{K_2 \cdot P}. \quad (4)$$

Equation (4) shows the concept of the comprehensive test method, from which the comprehensive safety factor K_c can be represented as follows:

$$K_c = K_1 \cdot K_2. \quad (5)$$

According to (1) to (5), the comprehensive method is advantageous because it considers not only the overloading effect of the dam but also the influence of decreasing strength of rock mass and structural planes. Thus, this method integrates the merits of the overloading method and the strength reduction method.

2.2. Safety Factors of the Comprehensive Test Method. As shown in (5), the safety factor in the comprehensive test method is a product of the strength reduction coefficient K_1 and the overloading coefficient K_2. The strength reduction coefficient K_1 is the reduction factor of the mechanical parameters f and c, which mainly consider the softening effect of rock masses and structural planes under the actions of reservoir water. This situation occurs under the normal operation conditions of a dam. In the dam stability analysis, the degree of strength reduction for the structural planes is often assigned a value of 15%~30% according to engineering experiences [24]. Thus, the strength reduction coefficient K_1 is between 1.15 and 1.3 in the comprehensive model tests.

The overloading coefficient K_2 represents multiples of the design water pressure P, which can be withstood by the dam structure. The situation when the dam is subjected to an unusually large load is considered [25]. Obtaining the overloading coefficient K_2 in the comprehensive test method is very important. The deformation of the dam body and dam foundation directly reflects the dam stability and potential damage. Therefore, in a geomechanical model test, the monitoring results of the deformation of the dam and dam abutments should be analyzed in detail. In this study, the deformation catastrophe theory [26] is used to propose characteristic points of the deformation curves obtained from model tests, which provides a basis for evaluating the overloading coefficient. A typical curve between the dam deformation and the overloading coefficient of a dam model is shown in Figure 1.

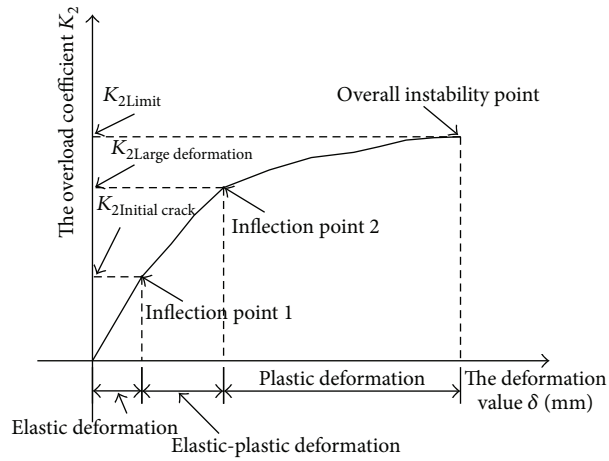

FIGURE 1: Typical curve between the deformation value δ and the overloading coefficient K_2 of a dam model.

Figure 1 shows that the failure process of a model dam can be divided into three stages, that is, the elastic deformation stage, the elastic-plastic deformation stage, and the overall instability stage. The curve has two inflection points. Before the first inflection point, the model is in the elastic deformation stage and the dam is in the normal operation phase. When the first inflection point approaches, the dam is assumed to have a small crack. At this point, the overloading coefficient K_2 is also called the initial cracking coefficient $K_{2\text{Initial crack}}$. As the overload continues to increase, the model dam enters the elastic-plastic deformation stage. In this stage, more and more cracks appear on the surface of the model dam but the dam structure remains stable. After the second inflection point is reached, the dam deformation increases suddenly and the model dam enters the plastic deformation stage. Finally, the entire model dam shows overall instability tendencies. In the model test, the second inflection point is called the large deformation inflection point, and the corresponding overloading coefficient is called $K_{2\text{Large deformation}}$. In addition, the overloading coefficient corresponds to the overall instability and is called $K_{2\text{Limit}}$. Based on the catastrophe theory and engineering practices [27], the second inflection point is critical for evaluating the stability of the model dam. In this study, the second inflection point of the deformation curve is considered as the indicator of the overloading coefficient $K_{2\text{Large deformation}}$.

2.3. Deformation Monitoring in the Comprehensive Method Test. In the comprehensive test method of geomechanical models, the measurement system of the model consists of three parts. The first part is to monitor the surface deformation of the dam and dam shoulders and the second part is to measure the strains of the dam. The third part is for monitoring the relative deformation of the internal structural planes in the abutment rock masses. Currently, linear variable differential transformers (LVDTs) are commonly used in modal tests to monitor the surface deformation. These instruments are based on Faraday's law of electromagnetic

induction and the sensing unit can convert the change of the measured signal to the change of mutual inductance. The transformer consists of a primary coil, a secondary coil, and an iron core. When an electric current passes through the primary coil, an initial voltage output is generated. This output causes the iron core to become mobile when the measured object moves, changing the mutual inductance coil. At this time, the output voltage varies with the change in the mutual inductance coil, which is proportional to the applied displacement. Consequently, the displacement measurement can be obtained. The SP-10A digital displacement measuring instrument is commonly used in geomechanical model tests. The instrument is characterized by its simple structure, high sensitivity, and easy installation. The measurement range of displacement is ±1 to ±50 mm, with an accuracy of 0.001 mm.

The monitoring instruments of strain and relative deformation are all based on the electrical resistance measurement technique. Resistance strain gauges are used as sensing elements, and the Wheatstone bridge principle is used for data collection. Commonly used equipment for data collection is the UCAM-70A and UCAM-8BL universal digital testing device. The surface and internal displacements of a model dam are directly related to the stability of the dam and foundation. Once the deformation of the model dam is captured, the evaluation of the health condition of the prototype structure can be carried out. In the following sections, the monitoring results of a comprehensive model test of the Jinping-I high arch dam are presented and the deformation and failure characteristics of this dam are discussed.

3. Jinping-I High Arch Dam

3.1. Project Background. The Jinping-I hydropower station is a large-scale cascade hydropower station in China, which is located on the main branch of the Yalong River in Sichuan Province. This hydropower project has a total capacity of 3600 MW. The maximum height of the concrete hyperbolic arch dam is 305 m, which is the tallest arch dam under construction in the world.

The watercourse of the site area is straight, and the river flows towards N25°E. The valley consists of deep V-shaped canyons with a relative elevation difference of 1500 m to 1700 m. The rock stratum of the left river bank is a reverse slope. The upper and lower rock strata are mainly composed of sandy slate and marble, respectively. The rock stratum of the right river bank forms a consequent slope, and the rock stratum consists of marble. The slope of the lower part is steep and the higher part is gentle. The typical geological profile of this site is shown in Figure 2.

The rock masses in the arch dam abutment are strongly affected by geological tectonics. Within the rock masses, faults, alteration veins, inner layer compressed zones, joint fissures, deep cracks, and other types of weak structural planes exist, which greatly influence the overall stability of the dam and foundation. The most critical geological structures include the following: (a) the faults f5, f2, f8, f42-9, f9, and F1; (b) the compressed zone g; (c) the lamprophyre dike X and deep cracks on the left bank; (d) the faults f13, f14, and f18; (e) the greenschist lens; and (f) the steep dip joints in the South-North (SN) direction on the right bank.

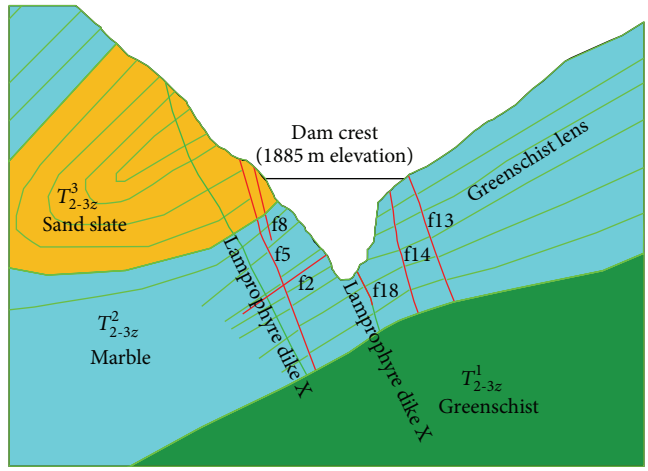

Figure 2: Typical geological condition at the Jinping-I arch dam site.

3.2. Reinforcement Measures of the Dam Abutment and Foundation. Because the geological conditions of the Jinping-I high arch dam are very complex, large amounts of reinforcements are needed to assure the stability of the dam and foundation. Considering the main geological structures and technical feasibility, the main reinforcement measures in this project include the following: (a) the concrete seating replacement in the left abutment; (b) the concrete replacement grids and hole-plugs for the weak structural planes; (c) the shearing resistant holes, the grooving replacement, and the consolidation grouting. For example, according to the development situation of the fault f2 and the compressive belt (g), grooving replacement was used in the foundation surface near an elevation of 1670 m, where f2 and g were intensively exposed and some of the fault f5 was replaced by two layers of flat holes and four inclined shafts of concrete. The lamprophyre dike X was replaced by three layers of concrete replacement holes and seven concrete replacement holes. Some of the left bank abutment was replaced by concrete cushion blocks at elevations of 1730 m to 1885 m, and three shearing resistant holes were set along the fault f42-9 at elevations of 1883 m, 1860 m, and 1834 m. Furthermore, five dowel holes were set up at elevations of 1829 m, 1785, m and 1730 m. In the right abutment, the concrete grooving replacement, the concrete grids, and the hole-plug replacement for the weak structural planes and the consolidation grouting were adopted as the main reinforcement measures. For example, five concrete inclined adits were adopted along the fault f13 at an elevation of 1601 m to the exposed place, and three layer flat concrete replacement holes and five concrete replacement deviated holes were used to reinforce the fault f14. According to the development of the fault f18 and the accompanying lamprophyre dike X, grooving replacement was used in the foundation surface near an elevation of 1580 m where f18 and X were intensively exposed. A diagram of the reinforcement measures is shown in Figure 3.

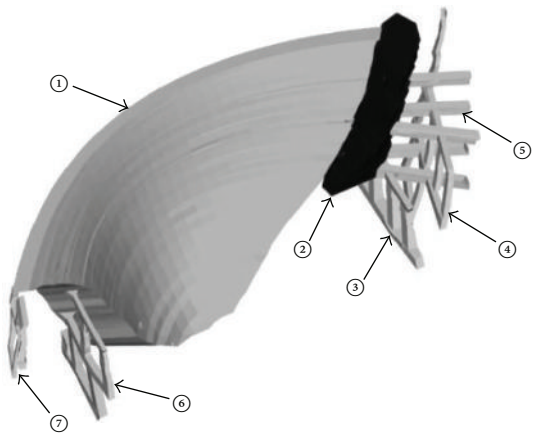

Figure 3: Schematic of the typical reinforcement measures used at the Jinping-I arch dam. ① The hyperbolic arch dam; ② the concrete seating replacement; ③ the concrete grids and hole-plug replacement for the fault f5; ④ the concrete grids and hole-plug replacement for the lamprophyre dike X; ⑤ the concrete shearing resistant holes; ⑥ the concrete grids and hole-plug replacement for the fault f14; ⑦ the concrete grids and hole-plug replacement for the fault f13.

4. Design of the 3D Geomechanical Model Test

4.1. Model Similarities and Mechanical Parameters of the Rock Masses and Structure Planes. A geomechanical model test is a type of destructive testing. According to the model similarity theory [28], the geomechanical model test must satisfy the following similar relationships: $C_\gamma = 1$, $C_\varepsilon = 1$, $C_f = 1$, $C_\mu = 1$, $C_\sigma = C_\varepsilon C_E$, $C_\sigma = C_E = C_L$, and $C_F = C_\sigma C_L^2 = C_\gamma C_L^3$. Here, C_E, C_γ, C_L, C_σ, and C_F are the deformation modulus ratio, the bulk density, the geometric ratio, the stress ratio, and the concentration force ratio, respectively. In addition, C_μ, C_ε, and C_f are Poisson's ratio, the strain, and the friction factor ratio, respectively. Combined with the practical engineering of the Jinping-I high arch dam, we selected a geometric ratio of $C_L = 300$, a bulk density of $C_\gamma = 1$, and model simulation dimensions of 4 m × 4 m × 2.83 m (river length × river width × height), which was equivalent to a region of 1200 m × 1200 m × 850 m in the prototype project. The load combination simulated in the test was performed based on the sum of the water pressure, the earth pressure, and the self-weight loads.

According to the physical and mechanical parameters of the arch dam concrete (the replacement concrete material), all types of rock masses, and the main structure plane materials provided by the designers, all types of physical and mechanical parameters can be obtained for the model materials by using a similarity relationship conversion. The main physical and mechanical parameters of the prototype and model materials are shown in Table 1.

4.2. Simulation of Rock Masses and Reinforcement Measures in the Dam Abutments and Foundation. In the geomechanical model test, the rock masses in the dam abutments and foundation were generally composed of small blocks of model materials that accurately simulated the nonlinear and multi-slit characteristics of the rock masses. Before the model test was performed, a large number of material tests were carried out based on the conversion of the mechanical parameters. The barite powder was the main material, and the high-grade engine oil was used as the cementing agent. They were mixed together at different proportions with additives to form the model material mixtures. Afterward, the model material mixtures were compressed using a BY −100 semiautomatic molding machine and became small blocks with dimensions of 10 cm × 10 cm × (5~7) cm (length × width × height).

In the geomechanical model, the arch dam, the left abutment concrete seating replacement, the concrete replacement, and other concrete materials were made from the mixtures of barite powder, gypsum, water, and small amounts of additives. The mixing proportions of the additives were selected according to the mechanical parameters of the model material. The model materials for the prototype concrete were molded according to the similarity relations.

4.3. Development of Temperature Analogous Materials for the Main Structural Planes. In this experiment, the main structural planes that affect the stability of the dam abutment were simulated, such as the faults f2, f5, f42-9, and F1, the lamprophyre dike X, the interlayer extrusion fault zone at the left-bank abutment, the faults f13, f14, and f18, and the greenschist lens at the right-bank abutment. To adopt the comprehensive test method and determine the influence of the main weak structural planes, a type of temperature-analogue material was developed to realize a gradually decreasing process of shear strength of the model material. Using this material, shear strength decreasing of the main faults f2, f5, f13, f14, and f18 and the lamprophyre dike X can be accurately controlled. The other structural planes were simulated using traditional model materials without adding polymer materials and additives and were produced by filling compaction with different thicknesses and mixing proportions. The mechanical parameters of the temperature-dependent analogous material are provided in Table 1. The relationships between shear strength and temperature were obtained using a series of shear tests, as shown in Figure 4. Prior to the test, the temperatures of the materials were calculated using the following equations: $\tau = 0.0001T^2 - 0.0177T + 1.131$ and $\tau = 0.0001T^2 - 0.1167T + 4.2714$. During the test, the shear strength of the temperature-analogue material was accurately reduced through a temperature control system.

When testing the shear strength indexes of the rock mass and the structural plane (f and c), we generally considered the combined effects of the shear strength as $\tau = f + c\tau = \sigma f + c$ because the friction factor ratio is $C_f = 1$ with a cohesion ratio of $C_c = C_\gamma \cdot C_L$ (where C_L is the geometric ratio and C_γ is the bulk density ratio). Thus, the modeled material cohesion c_m of conversion is very small, and the influences of cohesion c_m have often been neglected in previous experiments. Generally, the friction coefficient f_m of the geomechanical model material is smaller and the cohesion c_m is larger. Thus, the value of cohesion c_m is virtually increased, which greatly affects the test results.

Table 1: Main physical and mechanical parameters of the prototype and model materials.

Types of material	μ_p	E_p (10^3 MPa)	f_p	c_p (MPa)	μ_m	E_m (MPa)	f_m	c_m (MPa)
Arch dam concrete (natural foundation)	0.17	24	1.4	2.0	0.17	80.00	1.4	0.0067
Arch dam concrete (reinforcement foundation)	0.17	34	1.7	5.0	0.17	113.33	1.7	0.0167
Replacement concrete	0.17	31	1.5	3.5	0.17	103.33	1.5	0.0117
II class of rock mass	0.2	26.5	1.35	2	0.2	88.33	1.35	0.0067
III_1 class of rock mass	0.25	12	1.07	1.5	0.25	40.00	1.07	0.0050
III_2 class of rock mass	0.27	8	1.02	0.9	0.27	26.67	1.02	0.0030
IV_1 class of rock mass	0.3	3.5	0.7	0.6	0.3	11.67	0.7	0.0020
IV_2 class of rock mass	0.3	2.5	0.6	0.4	0.3	8.33	0.6	0.0013
V_1 class of rock mass	0.3	0.45	0.3	0.02	0.3	1.50	0.3	0.0001
Fault f2 (compressive zone g)	0.38	0.4	0.3	0.02	0.38	0.0013	0.3	0.0001
Fault f5	0.38	0.4	0.3	0.02	0.38	0.0013	0.3	0.0001
Fault f42-9	0.38	0.4	0.3	0.02	0.38	0.0013	0.3	0.0001
Lamprophyre dike X (fresh)	0.28	6.5	0.9	0.64	0.28	0.0217	0.9	0.0021
Lamprophyre dike X (weathering)	0.30	3.0	0.4	0.065	0.30	0.0100	0.4	0.0002
Fault f13	0.38	0.8	0.3	0.02	0.38	0.0027	0.3	0.0001
Fault f14	0.38	0.5	0.3	0.02	0.38	0.0017	0.3	0.0001
Fault f18	0.38	0.5	0.3	0.02	0.38	0.0017	0.3	0.0001
Greenschist lens	0.30	3.0	0.6	0.15	0.30	0.0100	0.6	0.0005

Note: ① μ, E, f, and c are Poisson's ratio, deformation modulus, friction coefficient, and cohesion, respectively; ② the subscript m represents a similarity model and the subscript p represents a prototype.

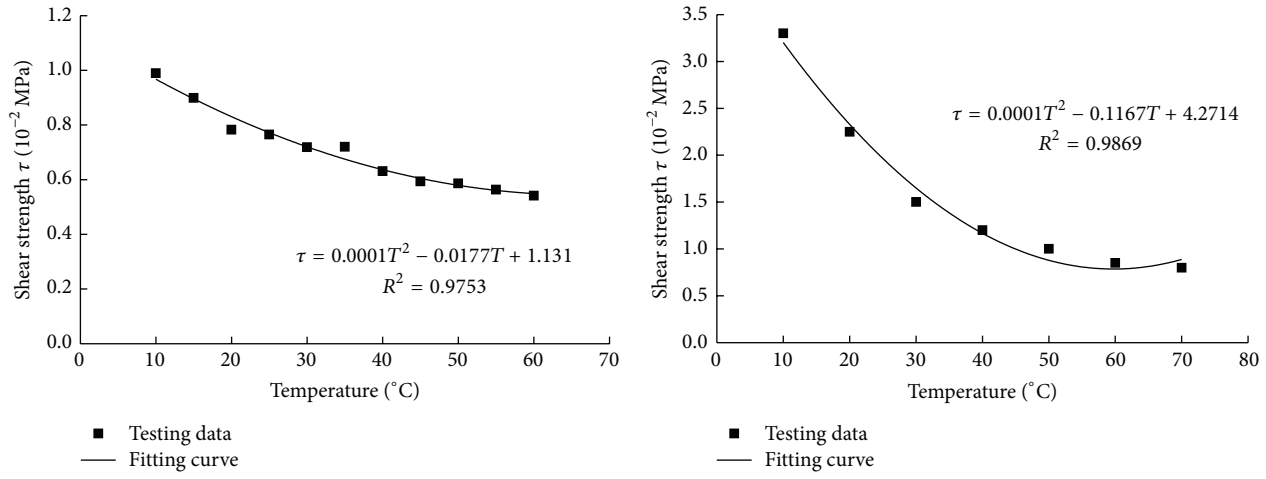

(a) Faults f2, f5, f13, f14, and f18 (faults fi)

(b) Lamprophyre dike X

Figure 4: Shear strength ~ temperature curve of the temperature analogous material.

If the combined effects of the two factors are considered by making the shear strength τ_m of the model material meet similar requirements, we will make the model results correspond more with practical engineering. Thus, in this 3D geomechanical model test of the Jinping-I high arch dam, the strength reduction stage test was conducted by considering the lower shear strength τ_m.

4.4. Model Construction. The geomechanical model was made of small masonry blocks. The position of the geological structures in the dam abutment and foundation was mainly dependent on the geological sliced figures, and the vertical and horizontal geological profiles determined the dip directions and dip angles. The model dam body and its reinforcement were placed and bonded to each other in

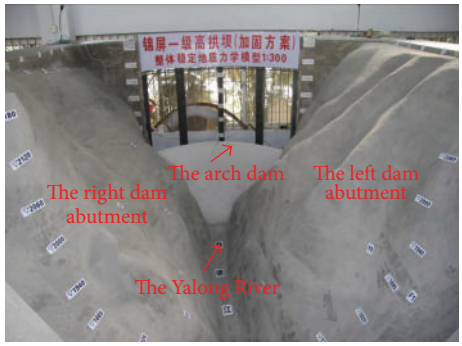

Figure 5: Photograph of the 3D geomechanical model of the Jinping-I arch dam.

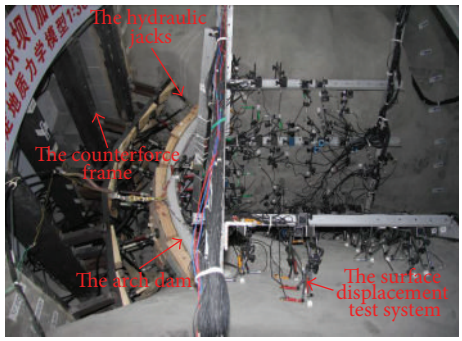

Figure 6: Arrangement of the loading system on the upstream surface of the model dam and the measurement system for the two dam shoulders.

steps. The internal relative displacement transducers and the temperature control system were installed during the model construction process. After the model was built, the model was refined according to the similarity scales. An overall view of the geomechanical model after completing the model refinement is shown in Figure 5.

4.5. Model Loading System. The load combination simulated in the test consisted of the water pressure, the earth pressure, and the self-weight load. Because the bulk density ratio $C_\gamma = 1$, the weights of the model and prototype materials are the same. In addition, the loading system applied the water pressure and earth pressure on the model dam through several layers of hydraulic jacks that were arranged on the upstream surface. By comprehensively considering the distributions of the water and earth pressures, the dimensions of the prototype dam, and the loading capacities of the loading system, the total load was divided into five layers. Meanwhile, the load of each layer was divided into several blocks. The calculated load on each block was applied at the block center using a servocontrolled hydraulic jack. The total load on the upstream surface of the model dam was divided into 24 blocks, and the loads were applied using 24 jacks. Several load-spreading boards were used to eliminate concentrated stress. A photograph of the loading system on the upstream surface of the model dam is shown in Figure 6.

4.6. Model Measurement System. In this model test, the requirements of the measurement data are mainly for the surface displacement and strain of the dam, surface displacement of the dam shoulders, and relative displacement of the internal structural planes in the abutment rock masses. Overall, 13 two-way or three-way deflection surface displacement measuring points for the downstream face of the dam were arranged at the elevations of 1880 m, 1830 m, 1750 m, 1670 m, and 1620 m to monitor the radial, tangential, and vertical displacements of the dam surface. 28 displacement transformers were installed to monitor the surface displacement and their data were collected by a SP-10A digital displacement measuring instrument. The arrangement of the surface deformation monitoring points on the downstream face is shown in Figure 7.

Overall, 15 strain measuring points were arranged on the downstream face of the model dam at the elevations of 1880 m, 1830 m, 1750 m, 1670 m, and 1620 m on the arch crown and arch abutment. Three resistance strain gauges were installed at every point to form a strain rosette. The strains at 0° direction (horizontal), 45° direction and 90° direction (vertical) were measured continuously using a UCAM-8BLuniversal digital testing device.

The surface displacements of 56 displacement monitoring points at the left and right dam abutments and the reinforcements were measured. To be specific, 33 measuring points were arranged on the left bank and 23 were arranged on the right bank. For every measurement point, the displacements of two opposite directions were automatically recorded by a SP-10A digital displacement measuring instrument. Therefore, there were a total of 112 displacement transformers. The arrangement of the surface displacement monitoring points of the left and right abutments and the reinforcements is shown in Figure 8.

Meanwhile, 88 relative displacement transducers were installed at the faults f13, f14, f18, f2, f5, f9, and F1, the lamprophyre dike X, the greenschist lens, and the SL15 deep cracks and at other weak structural planes to monitor the internal movement along the structures. Their readings were collected by a UCAM-8BL universal digital testing device.

5. Analysis of the Test Results

The 3D geomechanical model test was conducted for the Jinping-I high arch dam under reinforcement foundation conditions. First, a very small preloading was applied on the model dam. The normal load was applied afterward and remained constant. In the next stage, the shear strengths of the main structural planes were decreased gradually by heating the temperature analogous materials of the faults f2 and f5, the lamprophyre dike X in the left bank, and the faults f13, f14, and f18 in the right bank. The heating process was divided into six steps (from T1 to T6). The highest temperature was 50°C, which made the shear strength of the main structures reduce by approximately 30%. Then, the temperature level was maintained, and the loading was increased in stages using loading steps of 0.2~0.3 P (P is the design water pressure) until the model dam and foundation failed. During the test,

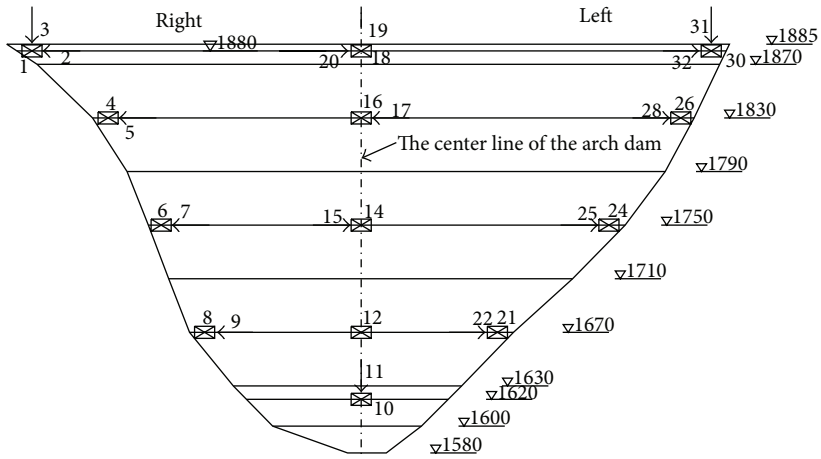

↓ represents the vertical displacement measuring point; the vertical upward deformation has a positive value.
⊠ represents the radial displacement measuring point; the downstream deformation has a positive value.
⟶ represents the tangential displacement measuring point; the deformation point to the left has a positive value.
10 represents the serial number of the deformation measuring point; total 28 displacement meters were installed.

Figure 7: Arrangement diagram for the surface deformation monitoring points of the downstream face of the arch dam.

the surface displacements, the internal displacements, and the strains of the geomechanical model were collected continuously. The monitoring data obtained in the test include the following: (a) the distributions of surface displacements of the dam structure and their development curves; (b) the distributions of surface displacements of the two abutments and the reinforcements and their development curves; (c) the distributions of relative displacements of the main faults, the lamprophyre dike and the weak structural zones in the dam foundation, abutment and reinforcements, and their development curves; and (d) the strain development curves of the model dam at typical heights. The failure processes and failure patterns of the abutment and the reinforcements were observed. The main results are presented and discussed as follows.

5.1. Analysis of the Displacements. The distribution characteristics of the dam displacement can be summarized as follows. (a) Under the normal or work load conditions, the dam displacements were almost symmetric. The maximum radial displacement was 80 mm (prototype value), which occurred at an elevation of 1880 m on the arch crown. (b) During the strength reduction phase and at the beginning of overloading, the dam displacements were small and the displacements of the left arch and right arch were still symmetric. (c) As the overloading increased, certain asymmetric displacements appeared, especially after K_2 = 4.0~4.6. The deformations at the left end of the arch obviously increased, and the displacements at the left end of the arch were slightly larger than the right arch. The left and right sides of the tangential displacement of the arch were roughly equal to each other throughout the loading process. The typical displacement curves are shown in Figure 9.

Many of the displacement curves indicate the following. (a) Under the normal load conditions with an overloading coefficient of K_2 = 1.0, the dam displacement was small. (b) During the strength reduction phase, the dam displacement curves slightly fluctuated, but the change was minor. (c) During the overloading phase, the deformation of the dam body gradually increased as the overload coefficient increased. (d) After the overload coefficient increased to 4.0~4.6, the slope of the displacement curves sharply changed, and the development of the displacements was accelerated. (e) When the overloading coefficient K_2 = 7.0~7.6, the dam deformation was very large, and the model arch dam and foundation had the tendencies of overall instability.

The distribution characteristics of surface displacements on the dam abutment and reinforcements can be summarized as follows. (a) The deformations near the end of the arch and near the exposed place of the lamprophyre dike X were generally larger than other areas. The deformation gradually decreased with the distance to the arch end. The typical displacement curve of the abutment is shown in Figure 10. Under normal load conditions and in the strength reduction phase, the surface displacements of the abutment and reinforcements were small, and the displacements of the left and right abutments were symmetrical. (b) During the overloading phase and before K_2 reached 4.0~4.6, the displacement gradually increased in a small magnitude. (c) After the overloading coefficient K_2 reached 4.6, the deformation of the abutment significantly increased as the overloading increases. This phenomenon indicates that large plastic deformation gradually occurred in the abutments and reinforcements. The displacements of the right bank were slightly larger than the left bank. Most of the displacement curves show an obvious turning point or a reduced slope between the overloading coefficients of K_2 = 4.0~4.6. When K_2 = 5.0~6.0, the slopes of the deformation curves further increased. (d) When K_2 = 7.0~7.6, the deformation of the abutment rock mass was very large. The surface cracks of

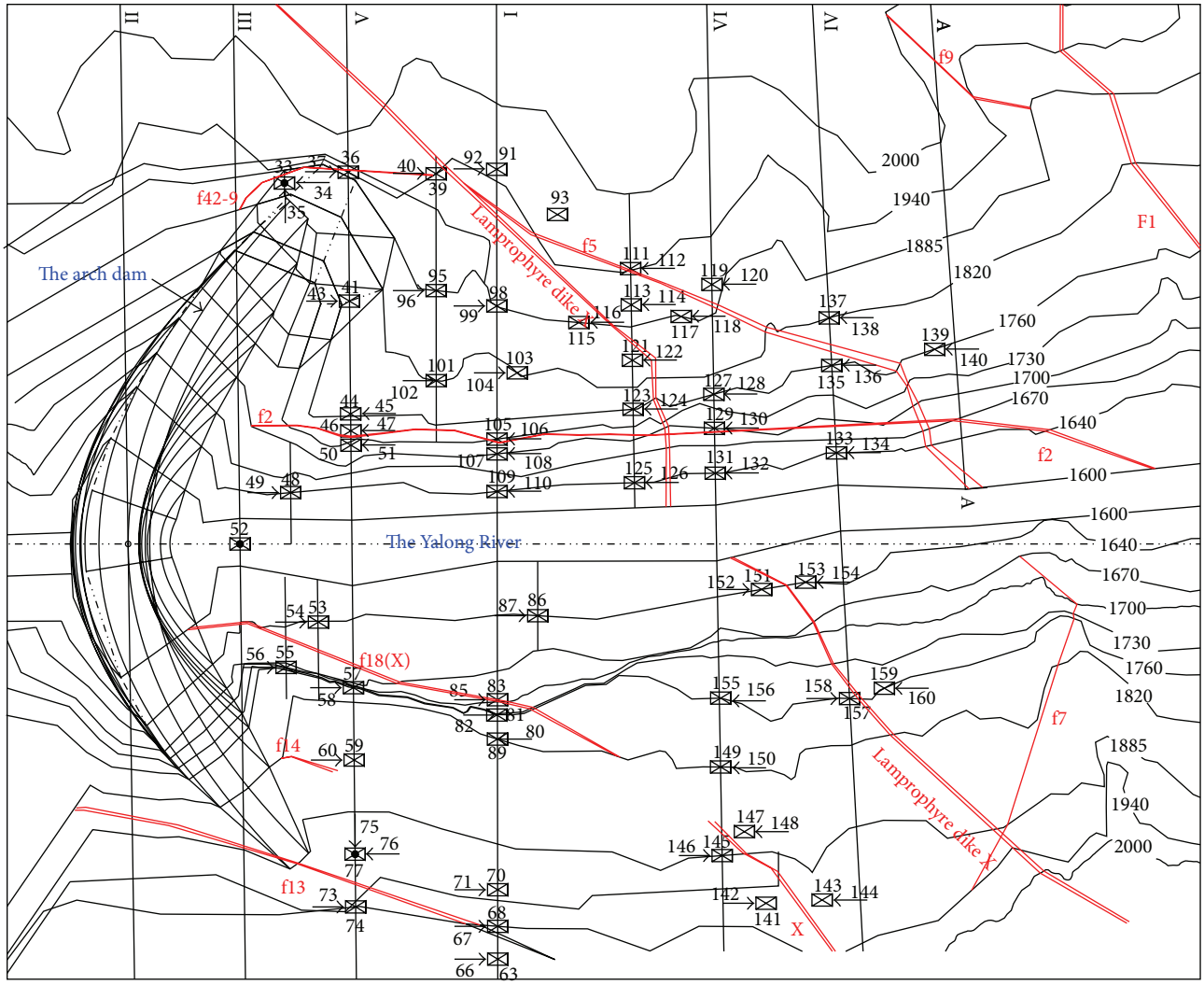

⟷ represents the displacement measuring point along river; the downstream deformation has a positive value.
⊠ represents the lateral displacement measuring point; to the river center deformation has a positive value.
40 represents the serial number of the deformation measuring point; total 112 displacement meters were installed.

Figure 8: Arrangement diagram for the surface deformation monitoring points of the left and right dam abutments.

the rock mass gradually propagated and connected with each other, and the abutment exhibited overall instability tendencies.

5.2. Analysis of Failure Processes and Failure Patterns. According to the observations, cracking of the model dam initiated at the dam heel when the overloading coefficient was K_2 = 1.4~1.6. When K_2 = 2.6~2.8, the abutment rock mass began to crack near the arch end of the dam crest at the faults f42-9 and f13. In addition, the fault f18 was exposed at its middle-lower portion. When K_2 = 4.0~4.6, the large deformation stage of the model dam was reached. The cracks of the two abutments increased and the dam heel crack significantly propagated and connected from the left to right. More and more cracks appeared and extended at the faults f42-9, f5, f2, f13, f14, and f18 and the lamprophyre dike X. The surface cracks increased in the middle portions of the two abutments and in the rock mass on the right bank near the dam crest. When K_2 = 7.0~7.6, the surface cracks in the left and right abutment rock masses were mutual intersections and were connected with each other. In addition, the model dam, the dam shoulder reinforcements, and weak structural planes demonstrated plastic instability. The final failure patterns of the model under the reinforcement foundation conditions are shown in Figures 11 and 12.

From the observations of the failure patterns, the following conditions are known. (a) After reinforcement, the final failure zones in the right abutment were mainly located in the triangle area from the fault f18 to the dam crest. This pattern mainly resulted from the interactions of cutting faults and steep dip cracks in the SN direction. Greenschist lenses were deposited in the middle portions of the right abutment,

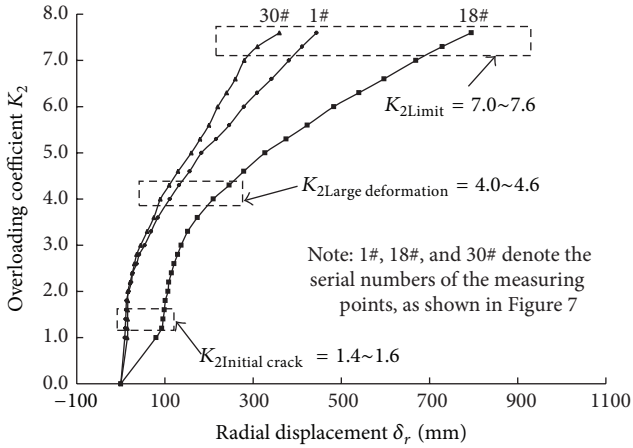

Figure 9: δ_r~K_2 relation curves regarding the radial displacement downstream at an elevation of 1880 m on the arch ring and the overloading coefficient.

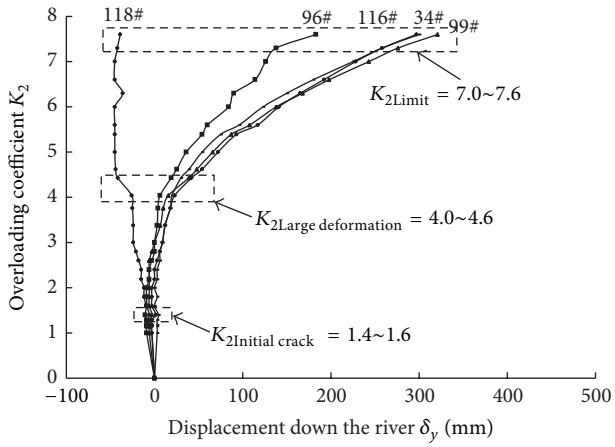

Figure 10: δ_y ~ K_2 relation curves regarding the deformation down the river at an elevation of 1885 m in the left bank and the overloading coefficient. Note: 34#, 96#, 99#, 116#, and 118# denote the serial numbers of the measuring points, as shown in Figure 8.

resulting in successive cracking at the faults f13, f14, and f18. The cracks in the rock masses expanded continuously in the steep dip direction of the fracture with mutual intersection and connectivity of the faults. (b) The final failure pattern of the left abutment is that the abutment significantly cracked along the structural planes of the faults f42-9, f5, and f2 and the lamprophyre dike X. These cracks were mainly due to the complex geological conditions of the left bank.

5.3. Analysis of the Overall Stability Safety Factor. Based on the geomechanical model tests, comprehensive evaluation of the overall stability and determination of the safety of the dam and foundation can be conducted based on the following five results: the surface displacement curves and strain curves of the dam body, the surface displacement curves of the reinforcements of the two dam shoulders, the internal relative displacement curves of the weak structural

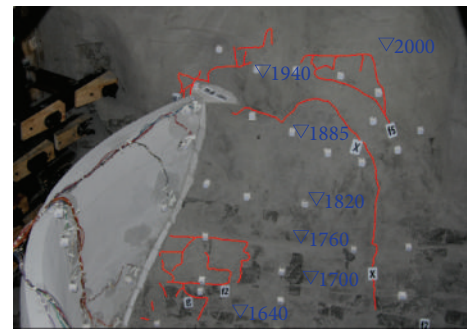

Figure 11: Failure patterns of the left abutment (K_2 = 7.6). Note: the red lines show the cracks in the model.

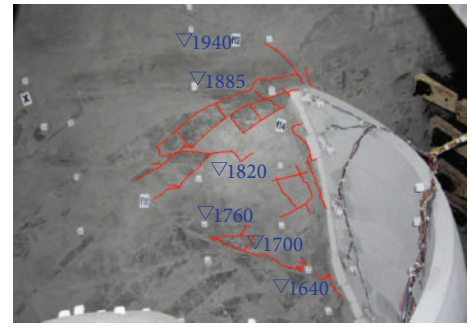

Figure 12: Failure patterns of the right abutment (K_2 = 7.6). Note: the red lines show the cracks in the model.

planes in the abutment rock masses, the observations of the deformation process and failure patterns of the abutments and the reinforcements, and the strength reduction magnitudes. According to the characteristics of the displacement curves, we can determine the strength reduction coefficient K_1 and the overloading coefficient K_2 of the arch dam and foundation. From the theory of the comprehensive test method, the comprehensive safety degree K_c can be represented as $K_c = K_1 \times K_2$.

The comprehensive analysis based on the information and results obtained from this experiment indicate that the Jinping-I high arch dam has a strength reduction coefficient of K_1 = 1.3 and an overloading coefficient of K_2 = 4.0~4.6. Thus, the comprehensive degree of safety of the Jinping-I high arch dam under reinforced foundation conditions should be $K_c = K_1 \times K_2$ = 5.2~6.0.

6. Conclusions

In this paper, a stability evaluation system for high arch dams based on deformation monitoring data obtained in comprehensive tests of geomechanical models was proposed. This method was used to investigate the overall stability of the Jinping-I high arch dam. Based on theoretical analysis and experimental investigations, the following conclusions were drawn.

(1) According to the basic principles of the three destructive test methods of geomechanical models and the basic concepts of point safety factors, an approach to assess the

stability and safety of dams was established based on the comprehensive geomechanical model test method.

(2) The stability evaluation system is presented based on the deformation monitoring data and the deformation-overloading coefficient curves. Based on the catastrophe theory and engineering practices, the second inflection point of the deformation curve is used to evaluate the stability of the model dam. An overloading coefficient $K_{2\text{Large deformation}}$ that corresponds to this inflection point is proposed. These results provide a theoretical basis for the comprehensive test method of geomechanical models.

(3) Using the comprehensive test method, a 3D geomechanical model test of the Jinping-I high arch dam under reinforced foundation conditions was conducted. During this test, the deformation characteristics, failure patterns, and mechanisms of the dam abutment and foundation were captured. The safety evaluation based on the experimental results indicates that the stability safety factors of the dam abutment and foundation range from 5.2 to 6.0. These research results have been applied in engineering. The proposed stability evaluation system in the context can be helpful for similar complex high arch dam projects.

Conflict of Interests

The authors declare that there is no conflict of interests regarding the publication of this paper.

Acknowledgments

This work was financially supported by the National Natural Science Foundation of China (nos. 51109152, 51379139, and 51409179) and Open Fund of State Key Laboratory of Hydraulics and Mountain River Engineering (Grant no. SKLGP2012 K011).

References

[1] J. Z. Pan and J. He, *Fifty Years of Chinese Dam*, China Water Power Press, Beijing, China, 2000, (Chinese).

[2] P. Bukenya, P. Moyo, H. Beushausen, and C. Oosthuizen, "Health monitoring of concrete dams: a literature review," *Journal of Civil Structural Health Monitoring*, vol. 4, no. 4, pp. 235–244, 2014.

[3] E. Fumagalli, *Statical and Geomechanical Models*, Springer, New York, NY, USA, 1973.

[4] X. H. Chen, *Structure Model Test for Brittle Material*, Water Resources and Electric Power Press, Beijing, China, 1984 (Chinese).

[5] X.-L. Yang, Z.-B. Wang, J.-F. Zou, and L. Li, "Bearing capacity of foundation on slope determined by energy dissipation method and model experiments," *Journal of Central South University of Technology*, vol. 14, no. 1, pp. 125–128, 2007.

[6] L. Zhang, B. Q. Yang, Y. Chen, C. Q. Hu, and J. H. Dong, "Measurement technology of structural plane displacement in deep sliding stability test of gravity dam," *China Science Paper*, vol. 9, no. 5, pp. 543–547, 2014 (Chinese).

[7] W. Huang and J. Chen, "Development of the internal displacement meter and the displacement observation automation used in structure model test," *Yangtze River*, vol. 6, pp. 19–20, 1997 (Chinese).

[8] H. H. Zhu, J. H. Yin, J. H. Dong, and L. Zhang, "Physical modelling of sliding failure of concrete gravity dam under overloading condition," *Geomechanics and Engineering*, vol. 2, no. 2, pp. 89–106, 2010.

[9] H.-H. Zhu, J.-H. Yin, L. Zhang, W. Jin, and J.-H. Dong, "Monitoring internal displacements of a model dam using FBG sensing bars," *Advances in Structural Engineering*, vol. 13, no. 2, pp. 249–261, 2010.

[10] W. S. Zhu, Q. B. Zhang, H. H. Zhu et al., "Large-scale geomechanical model testing of an underground cavern group in a true three-dimensional (3-D) stress state," *Canadian Geotechnical Journal*, vol. 47, no. 9, pp. 935–946, 2010.

[11] H. H. Zhu, A. N. L. Ho, J. H. Yin, H. W. Sun, H. F. Pei, and C. Y. Hong, "An optical fibre monitoring system for evaluating the performance of a soil nailed slope," *Smart Structures and Systems*, vol. 9, no. 5, pp. 393–410, 2012.

[12] S. C. M. Ho, L. Ren, H.-N. Li, and G. Song, "A fiber Bragg grating sensor for detection of liquid water in concrete structures," *Smart Materials and Structures*, vol. 22, no. 5, Article ID 055012, 2013.

[13] T. Guo, F. Liu, B.-O. Guan, and J. Albert, "Polarimetric multimode tilted fiber grating sensors," *Optics Express*, vol. 22, no. 6, pp. 7330–7336, 2014.

[14] C. Piao, J. Yuan, D. Wang, and P. Li, "A study on distribution measurement and mechanism of deformation due to water loss of overburden layer in vertical shaft," *Journal of Sensors*. In press.

[15] W. Y. Zhou, R. Q. Yang, and G. R. Yan, "Stability analysis system for large dams," *Chinese Journal of Rock Mechanics and Engineering*, vol. 16, no. 5, pp. 424–430, 1997 (Chinese).

[16] W. Zhou, R. Yang, Y. Liu, and P. Lin, "Research on geomechanical model of rupture tests of arch dams for their stability," *Journal of Hydroelectric Engineering*, vol. 24, no. 1, pp. 53–64, 2005 (Chinese).

[17] Y. R. Liu, F. H. Guan, Q. Yang, R. Q. Yang, and W. Y. Zhou, "Geomechanical model test for stability analysis of high arch dam based on small blocks masonry technique," *International Journal of Rock Mechanics and Mining Sciences*, vol. 61, pp. 231–243, 2013.

[18] L. Zhang, Y. R. Liu, and Q. Yang, "Evaluation of reinforcement and analysis of stability of a high-arch dam based on geomechanical model testing," *Rock Mechanics and Rock Engineering*, 2014.

[19] M. Peng, X. Y. Li, D. Q. Li, S. H. Jiang, and L. M. Zhang, "Slope safety evaluation by integrating multi-source monitoring information," *Structural Safety*, vol. 49, pp. 65–74, 2014.

[20] L. Zhang, Y. Chen, B. Q. Yang, J. Y. Chen, and C. Q. Hu, "A comprehensive testing method for global stability analysis of high arch dams," *Joumal of Rock Mechanics and Geotechnical Engineering*, vol. 4, no. 1, pp. 73–81, 2012.

[21] C. G. Li and L. Zhang, "Application of poikilothermic-similar material in structural model test," *Design of Hydroelectric Power Station*, vol. 11, no. 2, pp. 1–6, 1995 (Chinese).

[22] W.-P. Fei, L. Zhang, and R. Zhang, "Experimental study on a geo-mechanical model of a high arch dam," *International Journal of Rock Mechanics and Mining Sciences*, vol. 47, no. 2, pp. 299–306, 2010.

[23] Y. Chen, L. Zhang, G. X. Yang, J. H. Dong, and J. Y. Chen, "Anti-sliding stability of a gravity dam on complicated foundation with multiple structural planes," *International Journal of Rock Mechanics & Mining Sciences*, vol. 55, pp. 151–156, 2012.

[24] L. Zhang and J. Y. Chen, *The Engineering Application of Model Test about Hydraulic Dams and Foundation*, Sichuan University Press, Chengdu, China, 2009.

[25] N. H. Ru and Z. S. Jiang, *Arch Dams—Accident and Safety of Large Dams*, China Waterpower Press, Beijing, China, 1995 (Chinese).

[26] T. F. Bao, M. Xu, and L. Chen, "Stability analysis of concrete gravity dam foundation based on catastrophe model of plastic strain energy," *Procedia Engineering*, vol. 28, pp. 825–830, 2012.

[27] X. T. Ding, C. S. Gu, and Y. Jiang, "Analysis of stability of high arch dams based on FEM and catastrophe theory," *Journal of Hohai University (Natural Sciences)*, vol. 36, no. 2, pp. 175–178, 2008.

[28] X. S. He, H. Q. Ma, L. Zhang, and J. Chen, "Study of test method of geomechanical model and temperature analogous model material," *Chinese Journal of Rock Mechanics and Engineering*, vol. 28, no. 5, pp. 980–986, 2009 (Chinese).